

Supporting Information

Octanuclear Heterobimetallic {Ni₄Ln₄} Assemblies Possessing Ln₄ Square

Grid [2×2] Motifs: Synthesis, Structure and Magnetism

Sourav Biswas,^a Joydeb Goura,^a Sourav Das,^b Craig V. Topping,^c Jamie Brambleby,^d Paul A.

*Goddard^{*d} and Vadapalli Chandrasekhar^{*a,e}*

^aDepartment of Chemistry, Indian Institute of Technology Kanpur, Kanpur-208016, India.

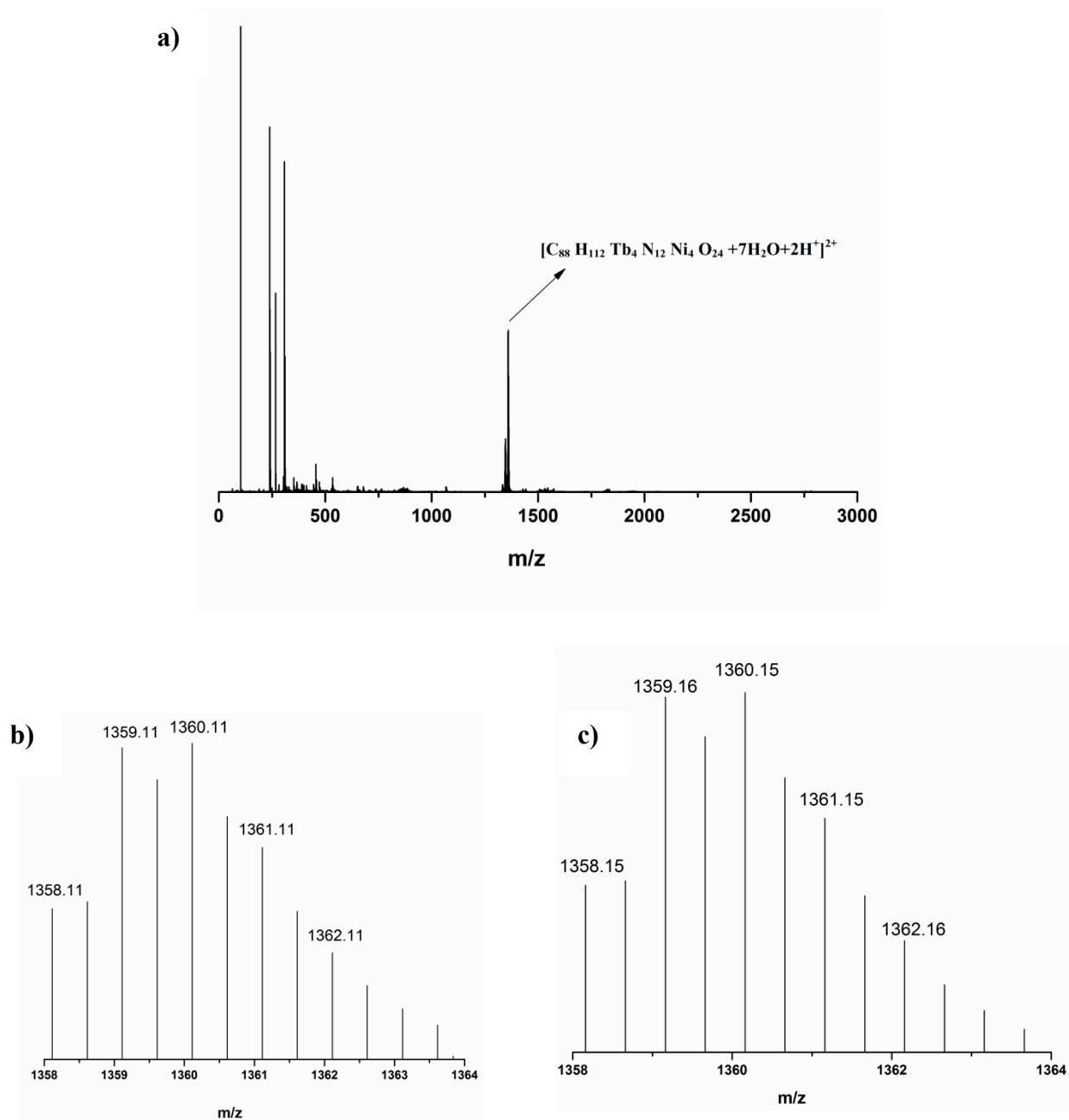
^bDepartment Of Chemistry, Institute of Infrastructure Technology Research and Management,
Near Khokhara Circle, Maninagar East, Ahmedabad-380026, India

^cClarendon Laboratory, University of Oxford, Parks Road, Oxford, OX1 3PU, United Kingdom.

^dDepartment of Physics, University of Warwick, Gibbet Hill Road, Coventry, CV4 7AL, United Kingdom.

^eNational Institute of Science Education and Research, Institute of Physics Campus,
Sachivalaya Marg, PO: Sainik School, Bhubaneswar - 751 005, Orissa, India.

AUTHOR EMAIL ADDRESS: vc@iitk.ac.in; vc@niser.ac.in; p.goddard@warwick.ac.uk



FigureS1. a) Full range ESI-MS spectrum of complex **2**. **b)** Experimental and **c)** Simulated mass spectral pattern of the species $[C_{88} H_{116} Tb_4 N_{12} Ni_4 O_{24} + 7H_2O - 2H^+]^{2+}$.

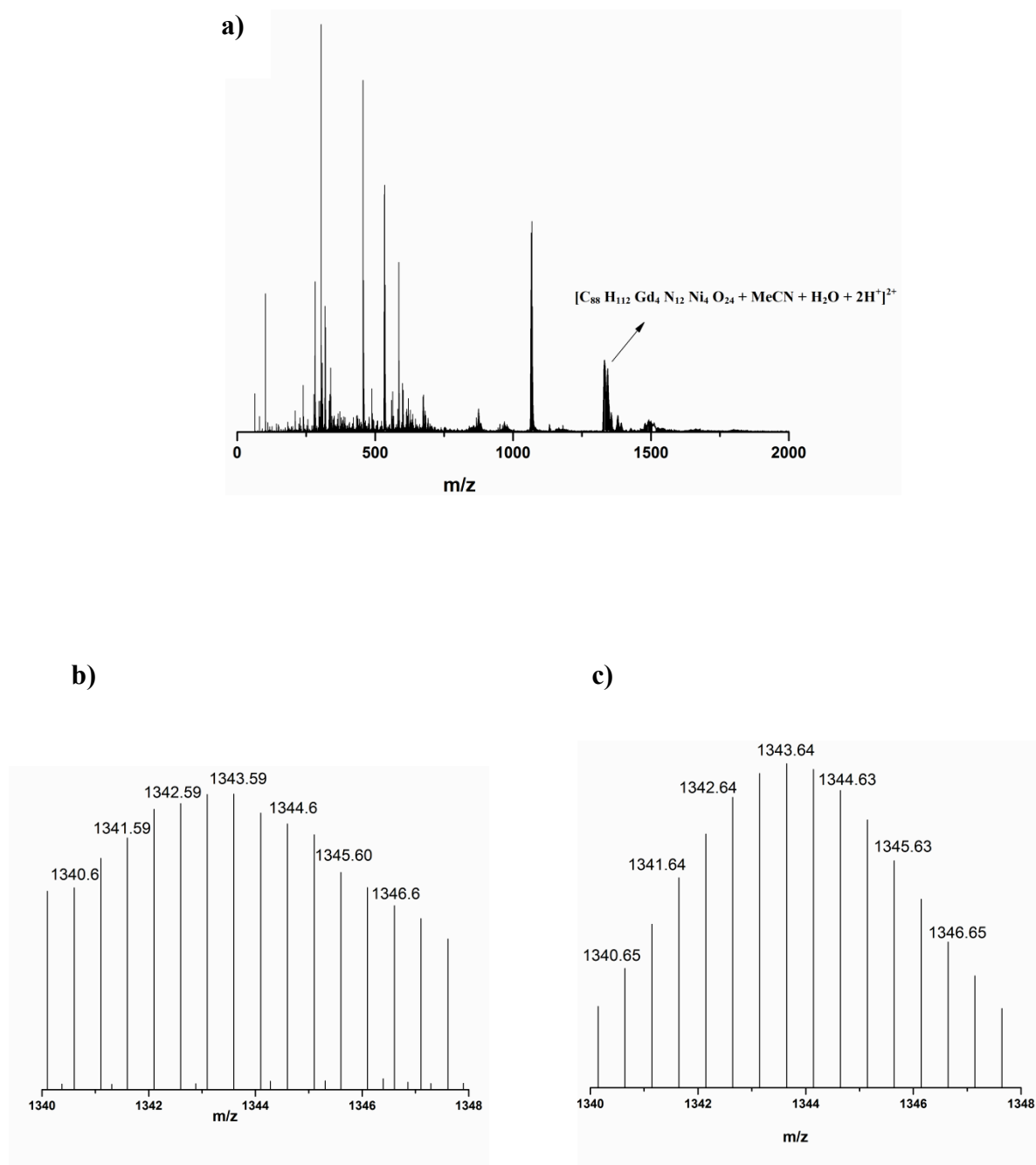


Figure S2. **a)** Full range ESI-MS spectrum of complex **3**. **b)** Experimental and **c)** Simulated mass spectral pattern of the species $[C_{88} H_{116} Gd_4 N_{12} Ni_4 O_{24} + MeCN + H_2O - 2H^+]^{2+}$.

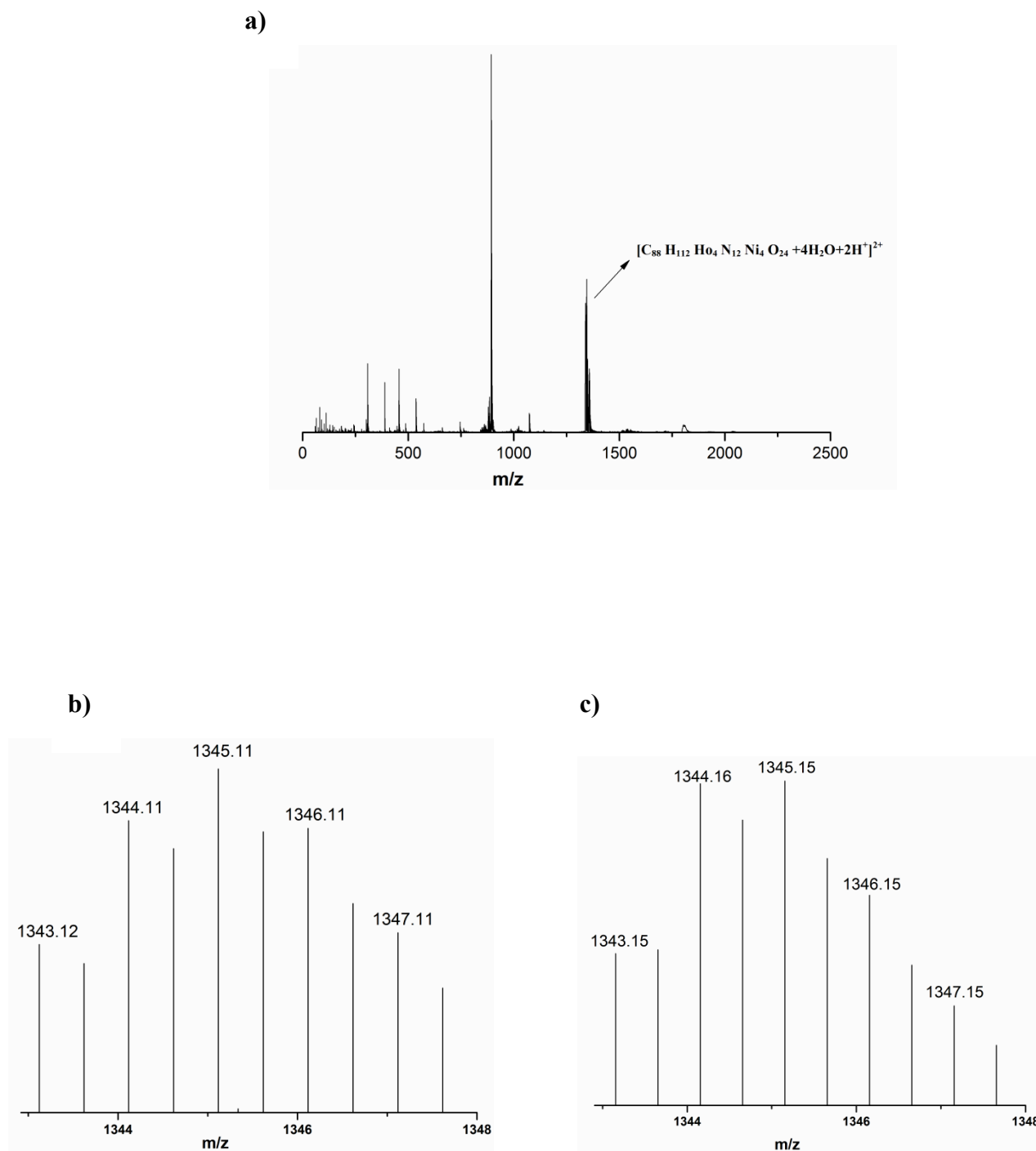


Figure S3.a) Full range ESI-MS spectrum of complex **4**. **b)** Experimental and **c)** Simulated mass spectral pattern of the species $[\text{C}_{88} \text{H}_{116} \text{Ho}_4 \text{N}_{12} \text{Ni}_4 \text{O}_{24} + 4\text{H}_2\text{O} - 2\text{H}]^{2+}$.

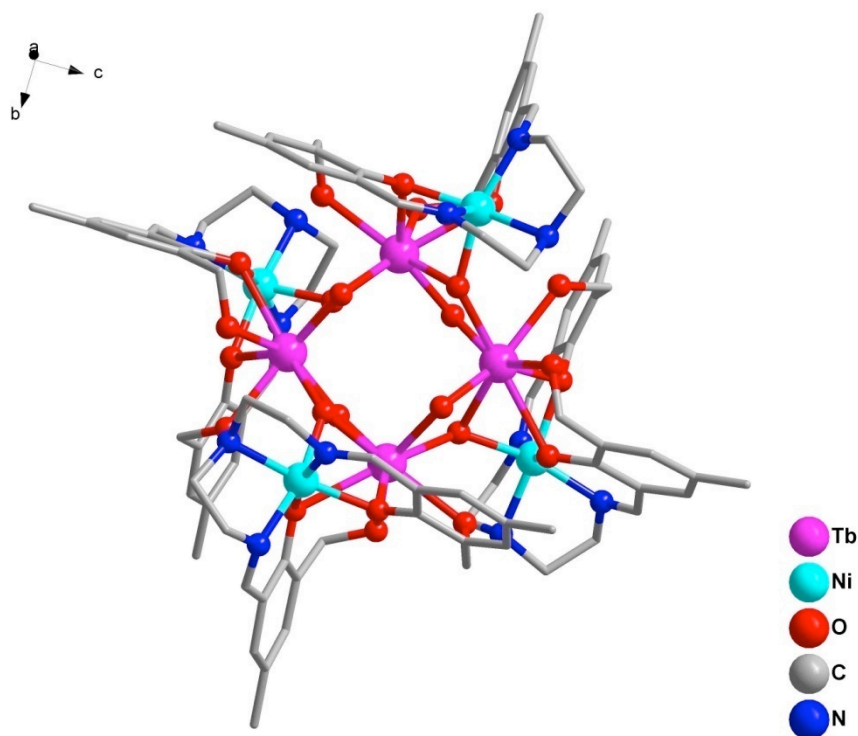


Figure S4. Molecular Structure of compound **2** (hydrogen atoms, chlorides and non coordinated solvent molecules were omitted for clarity).

TableS1. Selected Bond Distances (Å) and Bond angles (°) for compound**2**

Coordination environ around	Selected bond lengths	Selected bond angles
	Ni(1)-N(3) = 2.028(8) Ni(1)-N(1) = 2.046(8) Ni(1)-O(3) = 2.086(7) Ni(1)-O(5) = 2.100(7) Ni(1)-O(6) = 2.115(7) Ni(1)-N(2) = 2.164(9)	Ni(1)-O(5)-Tb(1)* = 139.2(3) Ni(1)-O(3)-Tb(1) = 92.3(2) Ni(1)-OH(6)-Tb(1) = 84.8(2)

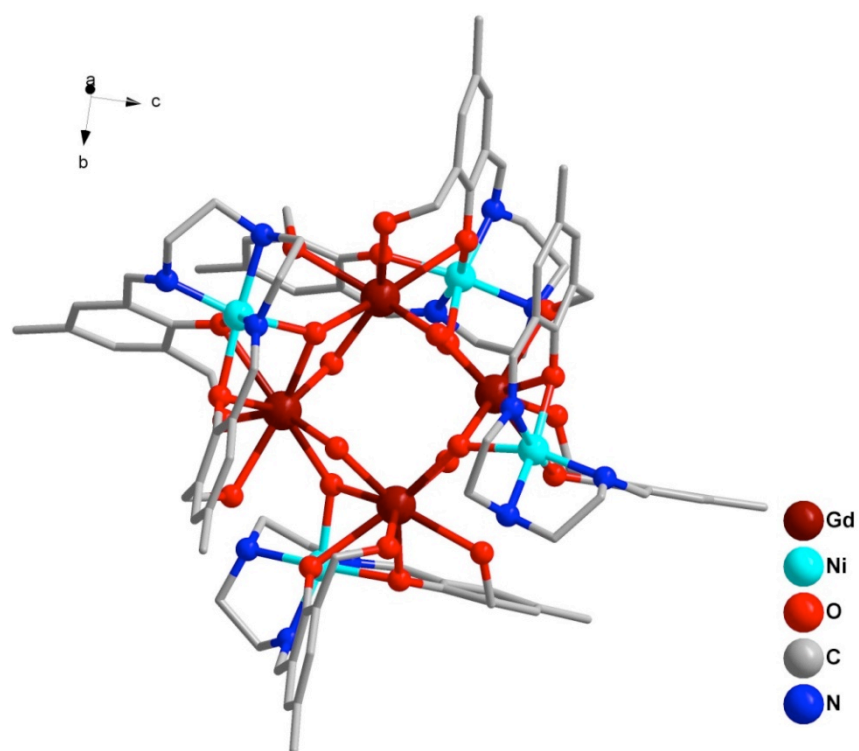
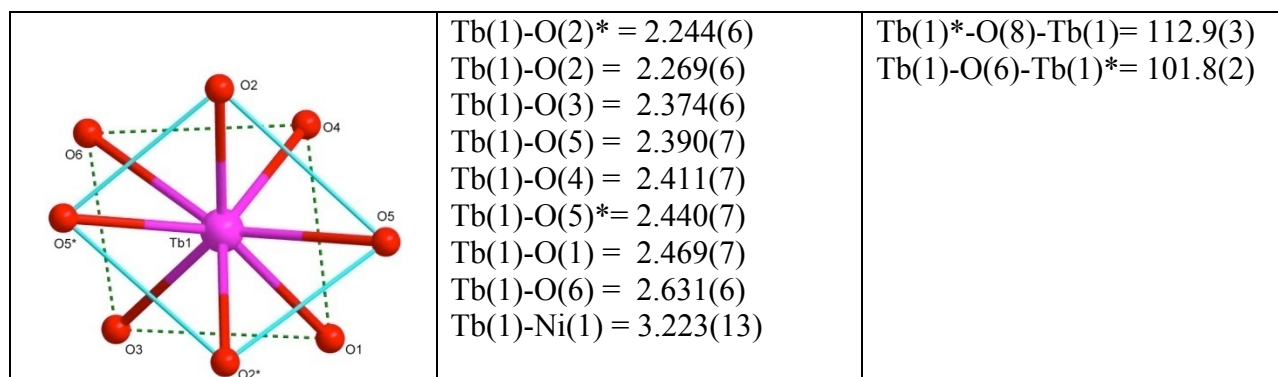
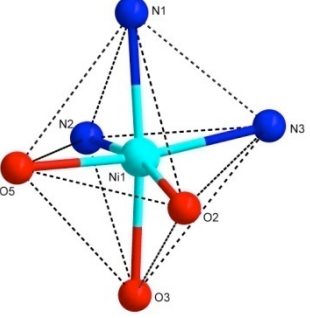
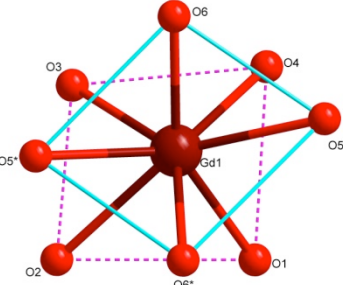


Figure S5. Molecular Structure of compound **3** (selected hydrogen atoms, chlorides and non-coordinated solvent molecules were omitted for clarity).

TableS2. Selected Bond Distances (Å) and Bond angles (°) for compound **3**.

Coordination environ around	Selected bond lengths	Selected bond angles
	<p> Ni(1)-N(3) = 2.014(9) Ni(1)-N(2) = 2.047(9) Ni(1)-O(3) = 2.090(7) Ni(1)-O(5) = 2.094(7) Ni(1)-O(2) = 2.115(7) Ni(1)-N(1) = 2.161(9) </p>	<p> Ni(1)-OH(5)-Gd(1) = 91.8(3) Ni(1)-OH(5)-Gd(1)* = 139.4(4) Ni(1)-O(3)-Gd(1) = 91.7(3) </p>
	<p> Gd(1)-O(6) = 2.250(6) Gd(1)-O(6)* = 2.290(7) Gd(1)-O(5) = 2.396(7) Gd(1)-O(3) = 2.405(7) Gd(1)-O(1) = 2.443(7) Gd(1)-O(5)* = 2.455(7) Gd(1)-O(4) = 2.501(7) Gd(1)-O(2) = 2.645(7) Gd(1)-Ni(1) = 3.232(14) </p>	<p> Gd(1)-O(6)-Gd(1)* = 112.7(3) Gd(1)-OH(5)-Gd(1)* = 102.4(3) </p>

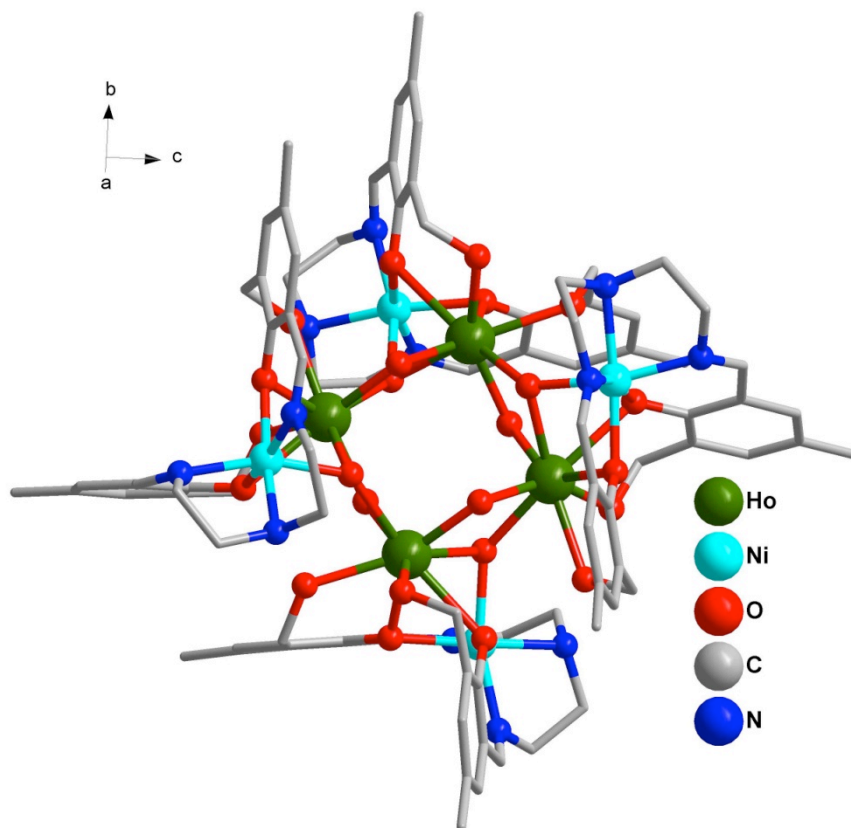
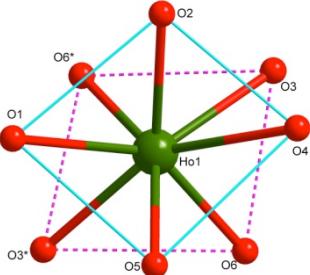


Figure S6. Molecular Structure of compound **4** (selected hydrogen atoms, chlorides and non coordinated solvent molecules were omitted for clarity).

TableS3. Selected Bond Distances (Å) and Bond angles (°) for compound **4**.

	<p> $\text{Ni(1)-N(2)} = 2.040(9)$ $\text{Ni(1)-N(3)} = 2.050(9)$ $\text{Ni(1)-O(2)} = 2.078(7)$ $\text{Ni(1)-O(4)} = 2.106(7)$ $\text{Ni(1)-O(3)} = 2.109(7)$ $\text{Ni(1)-N(1)} = 2.164(9)$ </p>	<p> $\text{Ni(1)-O(3)-Ho(1)} = 91.0(3)$ $\text{Ni(1)-O(3)-Ho(1)}^* = 138.5(3)$ $\text{Ni(1)-O(2)-Ho(1)} = 92.2(3)$ </p>
--	---	--

	$\text{Ho(1)-O(6)} = 2.223(7)$ $\text{Ho(1)-O(6)*} = 2.245(7)$ $\text{Ho(1)-O(2)} = 2.361(7)$ $\text{Ho(1)-O(3)} = 2.376(7)$ $\text{Ho(1)-O(5)} = 2.380(8)$ $\text{Ho(1)-O(3)*} = 2.425(7)$ $\text{Ho(1)-O(1)} = 2.445(7)$ $\text{Ho(1)-O(4)} = 2.599(7)$ $\text{Ho(1)-Ni(1)} = 3.204(14)$	$\text{Gd(1)-O(6)-Gd(1)*} = 112.7(3)$ $\text{Gd(1)-O(5)-Gd(1)*} = 102.4(3)$
---	--	--

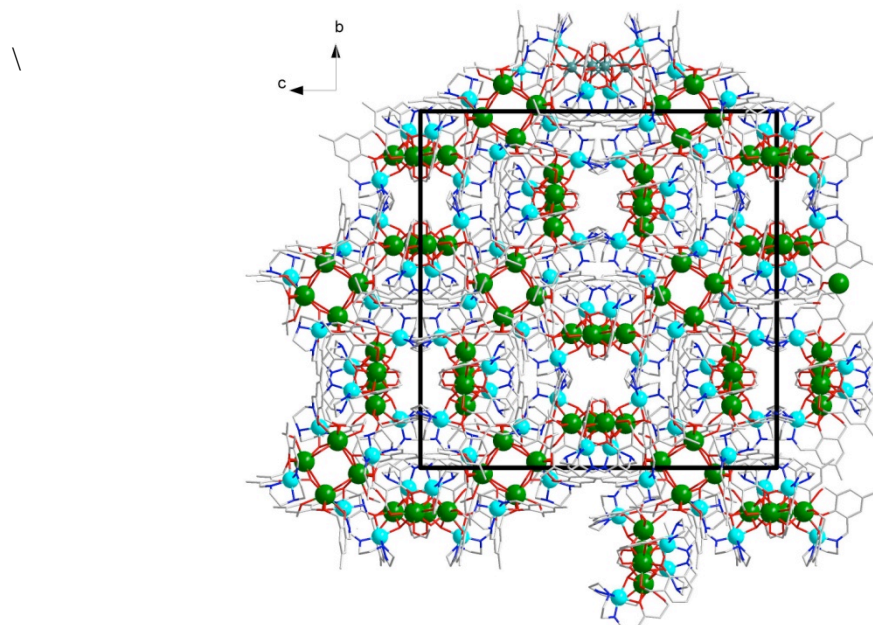


Figure S7. Crystal packing along the x axis.

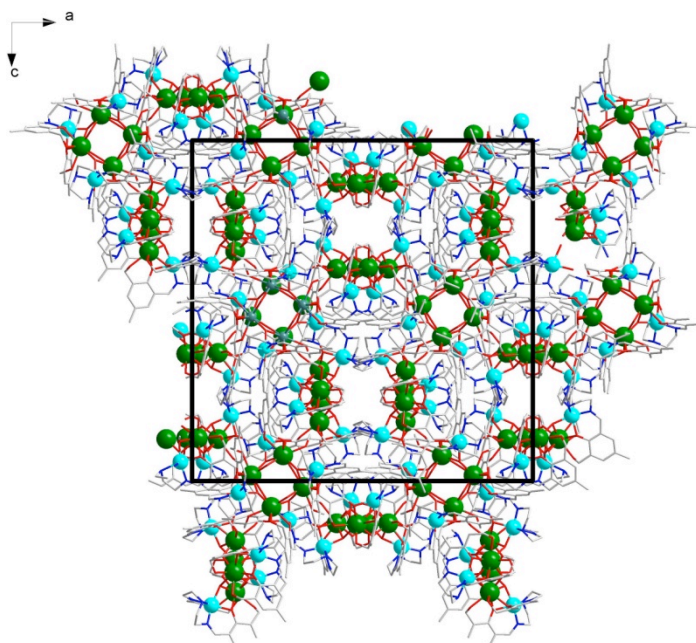


Figure S8. Crystal packing along the y axis.

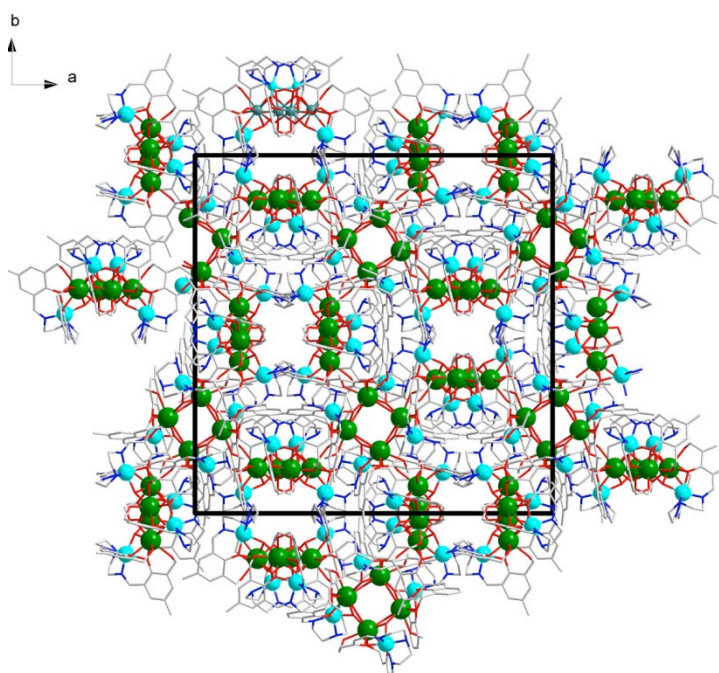


Figure S9. Crystal packing along the z axis.

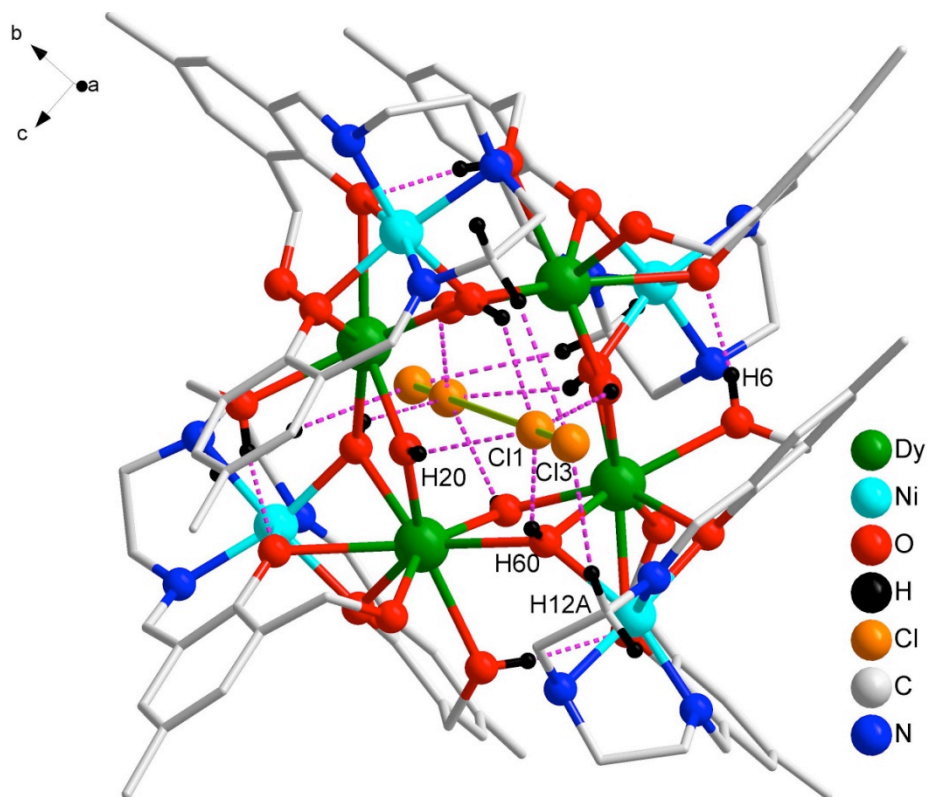


Figure S10. Molecular Structure of compound **1** (selected hydrogen atoms and non-coordinated solvent molecules were omitted for clarity).

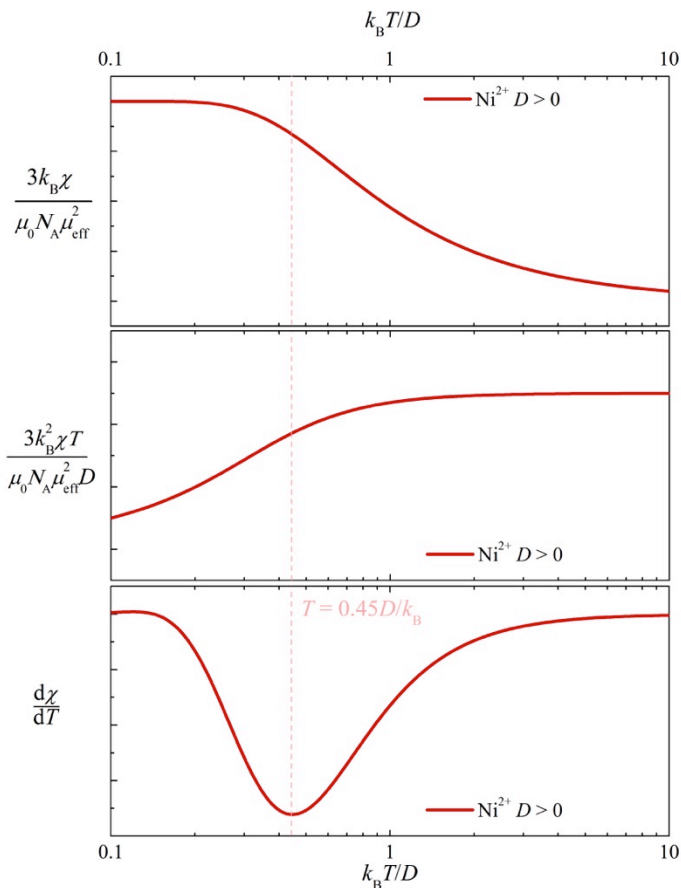


Figure S11. Simulated dc magnetic susceptibility curves of normalized χ , χT and $d\chi/dT$ against normalized temperature for Ni^{2+} ions of easy-plane single-ion anisotropy. A derived relation between the $d\chi/dT$ minimum and Ni^{2+} single-ion anisotropy, D_{Ni} , is indicated.

Magnetic properties

The susceptibility (χ) of an ensemble of spin-1 Ni^{2+} ions in an applied field (\mathbf{H}) was considered using the Hamiltonian

$$\mathcal{H} = D_{\text{Ni}} S_z^2 + g\mu_B\mu_0 \mathbf{S} \cdot \mathbf{H}, \quad (\text{S1})$$

where D_{Ni} is the single-ion anisotropy, S is the Ni^{2+} spin and g is the (isotropic) g -factor.

For a powdered sample, the susceptibility can be deduced from an exact diagonalization of Eq. S1¹ for fields applied parallel and perpendicular to the magnetic hard-axis (z), yielding

$$\chi = \frac{N_A\mu_0\mu_B^2g^2S(S+1)}{3} \left(\frac{e^{-\beta D}}{k_B T(1+2e^{-\beta D})} + \frac{2(1-e^{-\beta D})}{D(1+2e^{-\beta D})} \right),$$

where $\beta = 1/k_B T$ and $S = 1$ for Ni^{2+} in an octahedral coordination environment. The resultant susceptibility for $D_{\text{Ni}} > 0$ (Figure S11) indicates that a significant thermal depopulation of crystal-field split Ni^{2+} levels causes a decrease in the product χT on cooling concurrent with a pronounced minimum in $d\chi/dT$ centred at $T = 0.45D_{\text{Ni}}/k_B$.

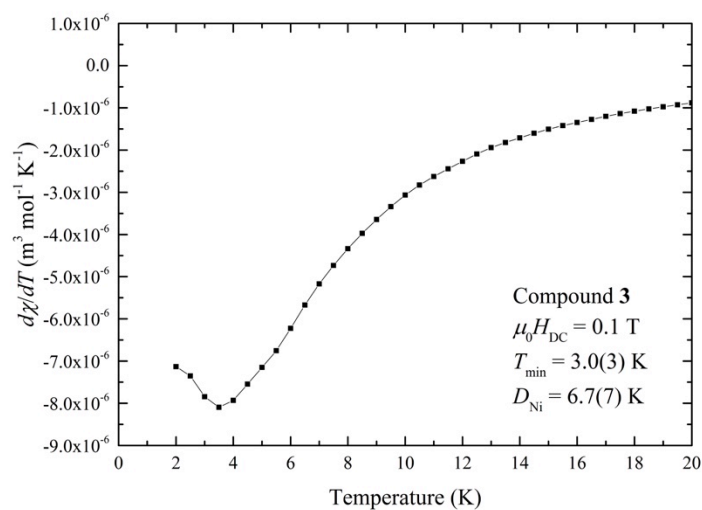


Figure S12. Dc magnetic susceptibility of **3** (Ni_4Gd_4) differentiated with respect to T , $d\chi/dT$, after interpolating data in 0.5 K steps and smoothing the resultant data via 3 point adjacent averaging. The minimum temperature is noted as well as the resultant D_{Ni} value via the relation from Figure S11.

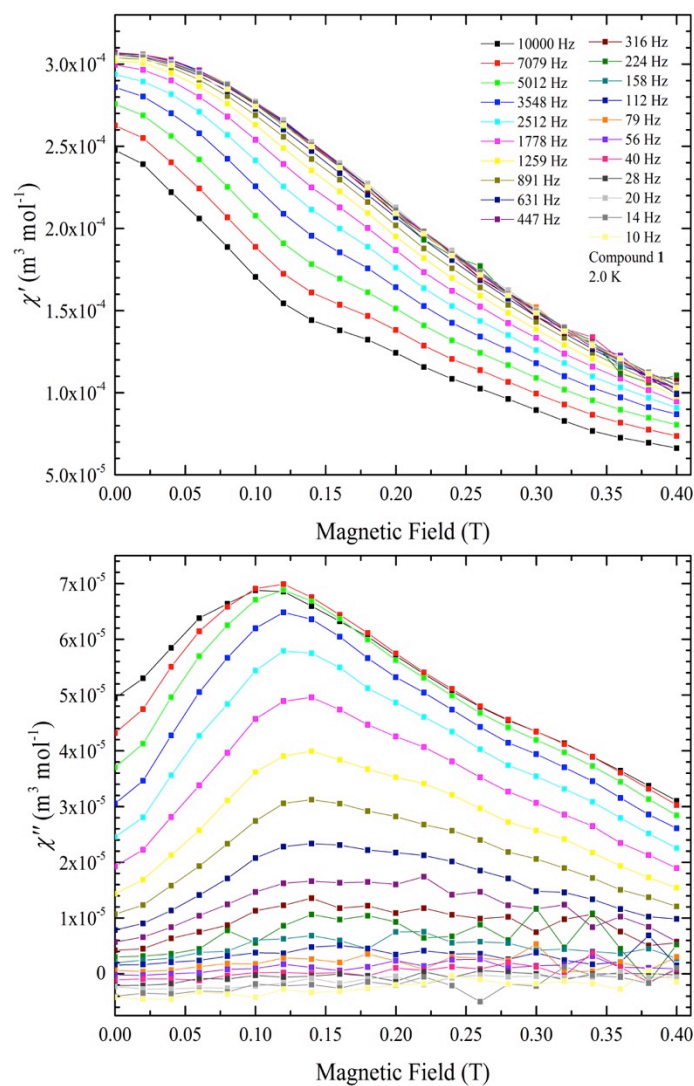


Figure S13. Magnetic field study of Ni_4Dy_4 at 2 K via ac susceptibility measurements. A dc magnetic field was increased from 0 T to 0.4 T in 0.02 T steps with a full set of frequencies measured at each step.

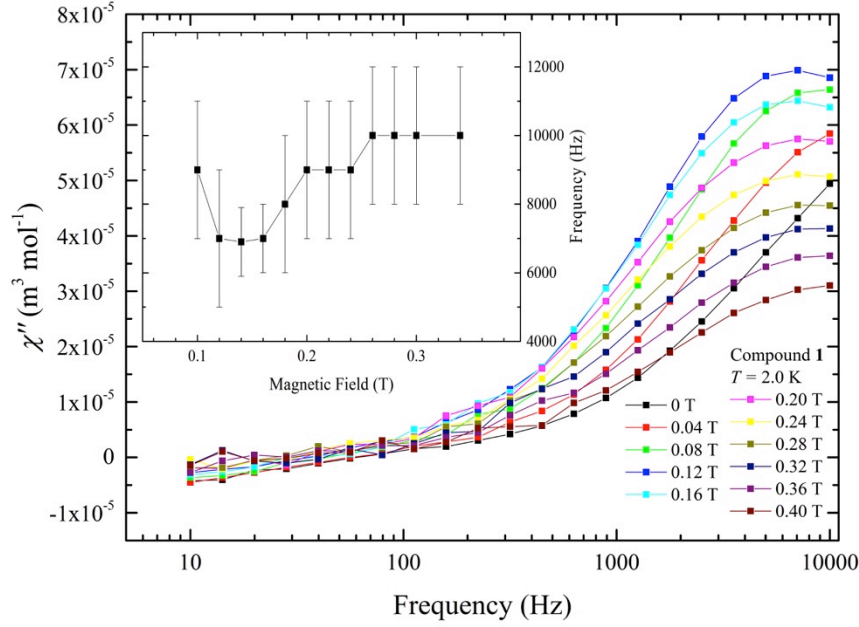


Figure S14. Out-of-phase susceptibility data from Figure S13 of Ni_4Dy_4 at 2 K plotted against frequency. Data at all magnetic fields approach a maximum at high frequencies. Inset: Frequency position of maxima χ'' plotted as a function of magnetic field.

When slow relaxation of magnetization is present in a system, the complex magnetic susceptibility may be described by the generalized Debye model:

$$\chi = \chi_s + \frac{\chi_T + \chi_s}{1 + [i\omega\tau(T)]^{1-\alpha}}, \quad (\text{S2})$$

where χ_s and χ_T are the adiabatic and isothermal susceptibility respectively, and $0 \leq \alpha \leq 1$ measures the spread of the relaxation time, τ .³² Rearranging the above to eliminate $\omega\tau$ results in²

$$\chi'' = -\frac{(\chi_T - \chi_S)}{2 \tan \left[\frac{\pi}{2} (1 - \alpha) \right]} + \sqrt{(\chi' - \chi_S)(\chi_T - \chi') + \frac{(\chi_T - \chi_S)^2}{4 \left(\tan \left[\frac{\pi}{2} (1 - \alpha) \right] \right)^2}}. \quad (\text{S3})$$

This slow relaxation may be detected in ac susceptibility data as a series of peaks in χ'' at the points at which the condition $\omega\tau = 1$ is satisfied.² For an organometallic cluster system τ may be expected to follow

$$\frac{1}{\tau} = aTB^2 + \frac{b}{1 + cB^2} + dT^n + \tau_0 e^{\frac{-U_{\text{eff}}}{kT}}, \quad (\text{S4})$$

where a , b , c , d and τ_0 are constants and B is the applied magnetic field.³ Each term represents a different possible relaxation process: direct, quantum tunnelling, Raman and Orbach processes respectively.³ SMM behavior is described by the Orbach term, which dominates other, none magnetic-field dependent terms in SMMs.⁴ To best detect the Orbach process, ac susceptibility measurements can be performed at the optimum dc magnetic field that minimizes the field-dependent terms. This is shown in the inset to Figure S14 in which the frequency position of the maxima in χ'' have been plotted against dc magnetic field. A minimum is seen at approximately $\mu_0 H_{\text{DC}} = 0.14$ T, which corresponds to the optimum field for the observation of SMM behavior in Ni_4Dy_4 .

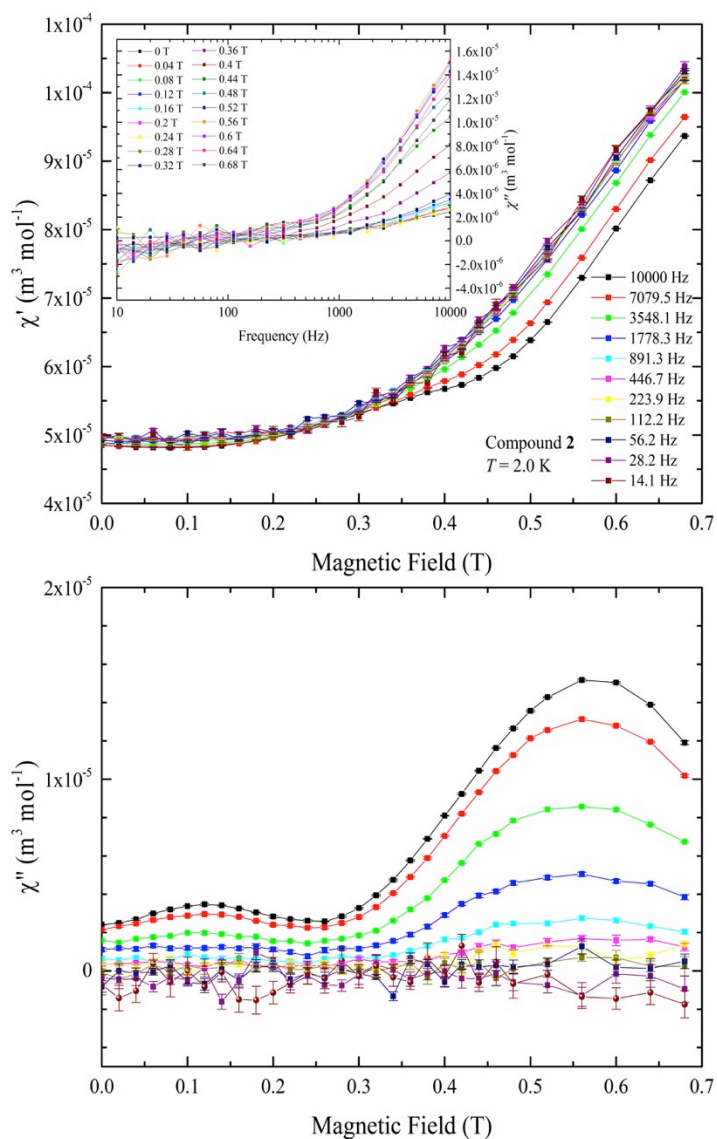


Figure S15. Magnetic field study of **2** (Ni_4Tb_4) at 2 K. A dc magnetic field was increased from 0 T to 0.68 T in initially 0.02 T steps before switching to 0.04 T steps above 0.48 T. Twenty-one frequencies were measured at each field. Only select frequencies are shown for clarity. Inset: out-of-phase susceptibility of Ni_4Tb_4 at 2 K plotted versus frequency. No maxima are visible within the accessible frequency range.

The field study of Ni₄Tb₄ (Figure S15) shows a number of differences compared to Ni₄Dy₄. χ' first decreases slightly on application of a magnetic field up to 0.1 T, before increasing more rapidly and displaying a marked frequency separation. A series of maxima are seen in χ'' in the low-field region at approximately the same fields at which χ' exhibits a minimum, with the higher frequency peaks occurring at slightly higher fields, which is in contrast to the maxima seen in the Ni₄Dy₄ material. As the dc magnetic field is increased, χ'' forms another, larger set of peaks. The χ'' data of Ni₄Tb₄ is plotted as constant field curves against frequency in the inset to Figure S15. This plot is very similar to the corresponding Ni₄Dy₄ plot (Figure S13). However, if maxima are to be observed in these data they lie outside the measured frequency range.

1) Molecular Magnetism, Kahn, O; Wiley-VCH, New York, **1993**.

2) Hagiwara, M. *J. Magn. Magn. Mater.* **1998**, 177, 89-90.

3) Novikov, V. V.; Pavlov, A. A.; Nelyubina, Y. V.; Boulon, M.-E.; Varzatskii, O. A.; Voloshin, Y. Z.; Winpenny, R. E. P. *J. Am. Chem. Soc.* **2015**, 137, 9792-9795.

4) Gatteschi, D.; Sessoli, R. *Angew. Chem. Int. Ed.* **2003**, 42, 268-297.